Atmos. Chem. Phys. Discuss., 10, 29631–29682, 2010
www.atmos-chem-phys-discuss.net/10/29631/2010/
doi:10.5194/acpd-10-29631-2010

Atmospheric Chemistry and Physics Discussions

SO_2 and BrO observation in the plume of the Eyjafjallajökull volcano 2010: CARIBIC and GOME-2 retrievals

K.-P. Heue[1], C. A. M. Brenninkmeijer[1], A. K. Baker[1], A. Rauthe-Schöch[1], D. Walter[1,3], T. Wagner[1], C. Hörmann[1,3], H. Sihler[1,3], B. Dix[2], U. Frieß[3], U. Platt[3], B. G. Martinsson[4], P. F. J. van Velthoven[5], M. Hermann[6], A. Zahn[7], and R. Ebinghaus[8]

[1]Max-Planck-Institut für Chemie (MPI), Mainz, Germany
[2]Department of Chemistry and Biochemistry, University of Colorado, Boulder, USA
[3]Institut für Umweltphysik, Universität Heidelberg, Heidelberg, Germany
[4]Avdelningen för kärnfysik, Lunds universitet, Lund, Sweden
[5]Koninklijk Nederlands Meteorologisch Instituut (KNMI), De Bilt, The Netherlands
[6]Leibniz-Institut für Troposphärenforschung, Leipzig, Germany
[7]Institut für Meteorologie und Klimaforschung (IMK) Karlsuhe Insitute of Technology, Karlsruhe, Germany
[8]Institut für Küstenforschung, GKSS, Geesthacht, Germany

Received: 20 October 2010 – Accepted: 24 November 2010 – Published: 6 December 2010

Correspondence to: K.-P. Heue (klaus-peter.heue@mpic.de)

ACPD
10, 29631–29682, 2010

Abstract

The ash cloud of the Eyjafjallajökull[1] volcano on Iceland caused closure of large parts of European airspace in April and May 2010. For the validation and improvement of the European volcanic ash forecast models several research flights were performed. Also the CARIBIC (Civil Aircraft for the Regular Investigation of the atmosphere Based on an Instrument Container) flying laboratory, which routinely measures at cruise altitude (≈11 km) performed three dedicated measurements flights through sections of the ash plume. Although the focus of these flights was on the detection and quantification of the volcanic ash, we report here on sulphur dioxide (SO_2) and bromine monoxide (BrO) measurements with the CARIBIC DOAS (Differential Optical Absorption Spectroscopy) instrument during the second of these special flights on 16 May 2010. As the BrO and the SO_2 observations coincide, we assume the BrO to have been formed inside the volcanic plume. Both SO_2 and BrO observations agree well with simultaneous satellite (GOME-2) observations. SO_2 column densities retrieved from satellite observations are often used as an indicator for volcanic ash. For SO_2 some additional information on the local distribution can be derived from a comparison of forward and back scan GOME-2 data. More details on the local plume size and position are retrieved by combining CARIBIC and GOME-2 data.

1 Introduction

Volcanic eruptions emit large amounts of ash and reactive gases into the atmosphere. Depending on the mass of ashes emitted, its height and the geographical position of the volcano, the influence on the atmospheric composition varies between local and global (e.g., Pinatubo 1991). As an explosive eruption of the Icelandic volcano Eyjafjallajökull (63° 37′ 48″ N 19° 37′ 12″ W) from 14 April to 24 May 2010 demonstrated, a modest

[1]Also referred to as: Eyjafjalla (e.g. Schumann et al., 2010), Eyjafjöll or Eyjafjoll (e.g. Ansmann et al., 2010).

ACPD
10, 29631–29682, 2010

volcanic eruption can have serious atmospheric consequences as large parts of the Western European airspace were closed. Satellite observations of Eyjafjallajökull's plume showed enhanced values of sulphur dioxide (SO_2) mainly after 19 April 2010. Sulphur dioxide is typically emitted by volcanoes and therefore often used as tracer for volcanic plumes and hence for volcanic ash (Carn et al., 2009). Moreover, volcanic bromine monoxide (BrO) was detected by satellite measurements close to Iceland but also further downwind, suggesting that bromine was emitted by the Eyjafjallajökull as well.

Here we present observations of SO_2 and BrO north of Ireland on 16 May 2010. Based on the combination of the DOAS CARIBIC data with GOME-2 satellite data additional information on spatial distribution details can be gained. The data were recorded during a special mission of the CARIBIC observatory (Civil Aircraft for the Regular Investigation of the atmosphere Based on an Instrument Container, http://www.caribic-atmospheric.com; Brenninkmeijer et al., 2007) deployed on board of a Lufthansa Airbus A340-600 passenger aircraft. Three special flights were aimed at a fairly complete observation of the volcanic plume by means of in situ trace gas and aerosol measurements, complemented by air and aerosol sampling. As the SO_2 and BrO column densities were below the detection limit during the first flight (20 April 2010, when the plume originated from the first eruption phase having low SO_2 emissions), and the DOAS instrument malfunctioned during the third (19 May 2010), we focus on the second flight. Besides the Lufthansa – CARIBIC measurement flights, other airborne measurements (e.g. Schumann et al., 2010) as well as ground based observations by lidar and ozone soundings were made (Ansmann et al., 2010; Flentje et al., 2010).

The chemical processes inside volcanic plumes have been studied for a long time. Since Bobrowski et al. (2003) detected large amounts of BrO downwind of the Soufrière Hills volcano (Montserrat) studies also target the chemistry of halogen compounds. An overview of the chemistry in the plumes of degassing volcanoes is given by von Glasow et al. (2009). While sulphur dioxide (SO_2) is directly emitted by volcanoes, bromine

ACPD
10, 29631–29682, 2010

monoxide (BrO) forms inside their plumes primarily through heterogeneous reactions (Eqs. R1–R5). The mechanism is similar to the one observed in polar spring leading to the "bromine explosion" and the concurrent arctic tropospheric ozone depletion events (e.g. Simpson et al., 2007). After attachment of HBr or HOBr to acidic aerosols, Br_2 is produced in the aqueous phase by the reaction with Br^- and H^+. Molecular bromine is released into the atmosphere, where it is photolysed and the bromine atoms react with O_3 to form BrO and O_2. Hence the production of BrO takes only place under daylight conditions. Moreover the mixing ratio of ozone must be sufficient through mixing in of background air from outside the plume. Other studies (Bobrowski et al., 2007) on volcanic BrO close to a crater observed a higher BrO concentration towards the plume edges compared to the centre. They concluded that the enhanced mixing in of ozone towards the edges caused the higher BrO concentration there, in contrast to the plume centre, where the ozone concentration is too low.

$$HBr \rightarrow HBr_{aq} \quad \text{(R1)}$$

$$HOBr_{aq} + Br^- + H^+ \rightarrow Br_{2,aq} + H_2O \quad \text{(R2)}$$

$$Br_{2,aq} \rightarrow Br_2 \quad \text{(R3)}$$

$$Br_2 \xrightarrow{h\cdot\nu} 2\cdot Br \quad \text{(R4)}$$

$$Br + O_3 \rightarrow BrO + O_2 \quad \text{(R5)}$$

$$BrO + BrO \rightarrow Br_2 + O_2 \quad \text{(R6)}$$

As the heterogeneous reaction of HCl is slower by several orders of magnitude (Sander et al., 1997) a corresponding chlorine explosion is not observed. However instead of Br_2 also BrX (X=F, Cl or I) may be released from the aerosols and become photo dissociated, leading to a small chlorine source. Indeed chlorine oxides (ClO, OClO) have been observed in volcanic plumes (e.g. Bobrowski et al., 2007). For the CARIBIC flight we report here, evidence for the presence of chlorine radicals will be presented elsewhere.

ACPD
10, 29631–29682, 2010

2 Description of the instruments

2.1 CARIBIC project

CARIBIC is based on a Lufthansa Airbus A340-600 retrofitted with a three probe (trace gases, water and aerosol) inlet system. Under normal operations the aircraft carries the instrument container on a monthly basis during four consecutive regular passenger flights for 2–3 days. CO, CO_2, O_3, NO, NO_2, NO_y, CH_4, some organic compounds (e.g. acetone), mercury, total and gaseous water and aerosols are measured in real time. In addition, 16 aerosol samples and 116 air samples (28 prior to spring 2010) are collected for post flight laboratory analysis of aerosol elemental composition, (Nguyen et al., 2006) and of a host of trace gases (Schuck et al., 2009; Baker et al., 2010a). A video camera in the inlet pylon takes a frame every second for post flight cloud cover analysis. Furthermore three miniature DOAS telescopes are mounted in the pylon. The instruments are maintained and operated by nine scientific groups from institutes in Europe (http://www.caribic-atmospheric.com, August 2010).

The instrumental container was updated in winter 2009/2010 with three new instruments: a new high resolution air sampler for 88 additional air samples, a cavity ring down absorption spectrometer (CRDS) for the D/H and $^{18}O/^{16}O$ ratios of water (Dyroff et al., 2010) and an off axis integrated cavity output spectrometer (OA-ICOS) for in situ measurements of CH_4 and CO_2 (Kattner et al., 2010). A new optical particle counter (OPC) for the aerosol size distribution between 125 nm and 1 µm was installed instead of the old one. The O_3 analyser, the H_2O instruments were improved and the NO_y instrument was extended for NO_2. Also the DOAS instrument was upgraded (Sect. 2.2).

The trace gas and aerosol measurements are complemented by standard in flight observations from the plane (e.g. position, temperature, wind speed, pressure) which are provided by Lufthansa. The Royal Dutch Meteorological Institute (KNMI) supports the CARIBIC project with trajectory calculations along the flight track based on the TRAJKS model (Scheele et al., 1996; Stohl et al., 2001). Both forward and backward trajectories for 2 and 8 days, respectively are calculated using ECMWF weather data

ACPD
10, 29631–29682, 2010

interpolated to the position and time of the CARIBIC observation.

2.2 DOAS on CARIBIC

The CARIBIC DOAS instrument is described in detail in Dix et al. (2009) and Heue et al. (2010). It measures scattered sunlight and uses Differential Optical Absorption Spectroscopy (DOAS) (Platt and Stutz, 2008) to retrieve trace gas amounts in the atmosphere. DOAS is based on the Lambert-Beer-Law:

$$I(\lambda) = I_0(\lambda) \cdot e^{\mathrm{SCD} \cdot \sigma(\lambda)} \quad (1)$$

It describes the reduction in the intensity I_0 at a certain wavelength (λ) when passing through a medium with absorption cross section ($\sigma(\lambda)$), with SCD being the absorber concentration (c) integrated along the light path:

$$\mathrm{SCD} = \int_{\mathrm{lightpath}} c(r)dr \quad (2)$$

It is usually referred to as Slant Column Density (SCD). Since many atmospheric trace gases e.g. NO_2, SO_2, BrO, O_3, O_4 or HCHO have unique absorption cross sections in the UV/Vis wavelength range, several tracers can be quantified simultaneously when using a certain wavelength interval. In principle the determination of SCDs requires knowledge of the solar radiation I_0 before entering the atmosphere. However, as this cannot be measured with the same instrument and the strong Fraunhofer absorptions have to be removed, a reference spectrum is included in the retrieval. Usually a normal scattered light spectrum recorded before or after the period of interest is used. Because of that the retrieved slant column is a differential column, relative to the reference spectrum. If possible a cloud-free spectrum from a clean part of the atmosphere is chosen as reference spectrum, since the subtracted column density is low in this case. In this study we used a cloudy spectrum recorded shortly after crossing the plume (10:35 UTC), assuming that the cloud coverage and optical density are similar

ACPD
10, 29631–29682, 2010

to those below the plume. For some trace gases, e.g. BrO, the subtraction of the reference spectrum automatically includes the correction for the stratospheric signal, if the change in the solar zenith angle is small enough.

As the slant column density is highly dependent on factors like viewing geometry, solar position, cloud coverage and aerosol content, the vertical column density is introduced to compare the observation with other data e.g. satellite observations. The vertical column density (VCD) is defined as the height integral of the concentration (Eq. 3). For the conversion of measured SCD to VCD an Air Mass Factor (AMF) is introduced as the ratio between SCD and VCD (Eq. 4). The AMF is numerically simulated under consideration of all above mentioned parameters. We used the radiative transfer model McArtim (Deutschmann, 2009), a full spherical Monte Carlo radiative transfer model, to retrieve the AMFs. Because of the Monte Carlo algorithm, the AMF has a statistical error. Together with the simulated AMF the 1σ variance is estimated by the program. For our study the error in the AMFs is below 7%.

$$\mathrm{VCD} = \int_0^{\mathrm{TOA}} c(z)\,dz \tag{3}$$

$$\mathrm{AMF} = \frac{\mathrm{SCD}}{\mathrm{VCD}} \tag{4}$$

The CARIBIC DOAS instrument observes scattered sunlight under three different elevation angles (-82°, named nadir, -10°, $+10^\circ$, relative to the horizon). The three small telescopes present in the CARIBIC-pylon are connected to the three spectrometers mounted in the container via quartz fibre bundles. In Winter 2009/2010 the existing Ocean Optic USB2000 spectrometers were replaced by new CTF60 spectrometers from OMT (optische Messtechnik, Ulm, Germany). The wavelength ranges of all spectrometers cover the interval from 300 to 400 nm with a spectral resolution of 0.5 nm (full width at half maximum). Hence it allows us to retrieve sulphur dioxide from all 3 lines of sight, in contrast to the old DOAS system (Heue et al., 2010). Moreover the

ACPD
10, 29631–29682, 2010

time resolution could be reduced from 30 to 8 s (corresponding to 7.5 km and 2 km horizontal resolution, respectively) without increasing the measurement errors.

Unfortunately during the same period the quartz fibres in the bundle connecting the +10° telescope with its spectrometer was damaged and could not be replaced before the volcanic flights. So, for this study only two viewing directions are active. Moreover since these were the first data recorded with the new system (immediately after the recertification of the CARIBIC container after the updates) some parameter settings were still suboptimal. Particularly the intensity detected with the −10° spectrometer is far below that of nadir and some spectra reached oversaturation since the determination of the integration time had to be optimized under real flight conditions. Apart from the high temporal resolution analyses of all spectra, occasionally up to ten spectra were co-added (excluding the oversaturated ones) to reduce noise and improve the detection limit.

The wavelength interval for the SO_2 analysis ranged from 311.6 nm to 333 nm (5 SO_2 bands) for comparison also the wavelength range down to 307.5 nm was considered, covering another SO_2 band. Due to strong absorption of UV light by stratospheric ozone, the signal strength deteriorates when extending the wavelength range to shorter wavelengths. For the same reason BrO was retrieved in a second fitting window, (324 to 353 nm) which includes 6 bands where the recorded intensity of the spectra is up to 3 times higher compared to the SO_2 interval. A third fitting window (332–367 mm) was added to retrieve the O_4 column density. It should be mentioned that similar SCDs were observed in the different wavelength intervals (except for a higher noise in the SO_2 fitting window).

Besides SO_2 (Bogumil et al., 2003, 273 K) and BrO (Wilmouth et al., 1999, 228 K), also O_3 (Bogumil et al., 2003, 223 K and 243 K) and NO_2 (Vandaele et al., 1996) were taken into account in the data retrieval. For the BrO and the O_4 fitting windows (Fig. 1) O_4 (Greenblatt et al., 1990) was included. To distinguish between the O_4 slant column densities (molec^2 cm^{-5}) and the normal SCD (molec cm^{-2}) the O_4 SCDs* are marked by an asterix. The filling-in of the Fraunhofer lines caused by inelastic scattering of

ACPD
10, 29631–29682, 2010

light (Grainer and Ring, 1962) was corrected by including a Ring spectrum (Bussemer, 1993; Kraus, 2005) in the retrieval. The Ring spectrum is calculated from the reference spectrum. Depending on the size of the fitting window a polynomial of third to fifth order was included to simulate the broad band effects like molecular scattering or aerosol scattering. The temperature in the plume was roughly −5 °C, hence the SO_2 cross section for 273 K is used for the SO_2 retrieval for CARIBIC and for GOME-2.

We also checked for OClO (Kromminga et al., 2003), which has already been observed in other volcanic plumes (e.g. Bobrowski et al., 2007). However, the resulting column density was always below the detection limit of 6×10^{13} molec cm^{-2} for the co-added spectra, corresponding to ≈4 ppt in the plume as described below (Sect. 4.1).

Formaldehyde (HCHO) is predicted by some models (R. von Glasow, personal communication, 2010) as product of enhanced methane oxidation caused by elevated chlorine concentrations. Although some retrieved column densities for HCHO approached the detection limit (1.5×10^{16} molec cm^{-2}), the respective DOAS fits were not robust as the retrieved columns showed a strong dependence on the choice of the wavelength range and the cross sections included in the retrieval. Assuming a plume height range from 3 to 6 km the retrieved SCD corresponds to an upper limit mixing ratio of roughly 1 ppb. HCHO results will not be further discussed.

In Fig. 1 an example fit for the three wavelength ranges (fitting windows) is shown, only a few trace gas absorptions are depicted here to keep the figure clear. The SO_2 absorption is very strong in this spectrum, but also the BrO absorption is clearly observed.

The typical fit error for BrO in the co-added spectra was around 1×10^{13} molec cm^{-2}, which is similar or slightly higher than depicted in Fig. 1. For the SO_2 the error in the SCD is in most cases less than 4×10^{15} molec cm^{-2} for the averaged nadir data. Due to the low optical density of BrO the relative measurement errors are higher. For the individual spectra the typical errors are 1.5–2×10^{13} molec cm^{-2} and 8×10^{15} molec cm^{-2} for BrO and SO_2, respectively in nadir and 6×10^{13} molec cm^{-2} and 2×10^{16} molec cm^{-2} for −10°, in the slant column density. The error of the vertical column density can be

ACPD
10, 29631–29682, 2010

calculated according to Eq. (4), whereby an error of the AMF of less than 7% can be assumed. Table 1 shows the total error of the vertical column density for both lines of sight and the important trace gases for this study.

2.3 GOME-2 on MetOp-A

A short description of the GOME-2 instrument and the SO_2 data retrieval is given in Heue et al. (2010). The GOME-2 (Global Ozone Monitoring Experiment) on MetOp-A is the first of a series of three identical instruments. MetOp-A was launched into a sun-synchronous polar orbit at 800 km altitude in October 2006 and crosses the equator at 09:30 LT (local time). The GOME-2 instrument is a 4 channel UV/Vis grating spectrometer, which covers the wavelength region of 240–790 nm with a spectral resolution of 0.2–0.4 nm. Besides the backscattered and reflected radiance from the Earth it also observes direct sunlight.

The ground pixel size is roughly $80 \times 40\,km^2$ and the total swath width is 1920 km (24 pixels wide), thereby achieving daily coverage at mid latitudes (http://www.esa.int/esaLP/LPmetop.html, September 2009). The respective pixels are scanned from the east to the west by rotating a mirror in the optical system of the entrance optics. When it turns back, the respective "back scan" pixel ($240 \times 40\,km^2$) is obtained. The forward and backward scan pixel partially overlap (Fig. 2). In Fig. 2 1/8 of the total swath is shown, it has 24 forward and 8 back scan pixels. The figure can be extended to both sides, and so the back scans shown here also partly overlap with the previous forward scans to the east, which are not shown.

The SO_2 absorption is analysed from the satellite spectra in the wavelength range from 312.1 to 324 nm (Fig. 1 left SO_2 window) using the DOAS method. To remove the Fraunhofer lines, a direct sun spectrum (containing no atmospheric absorptions) is included in the fitting process. The trace gas cross sections for O_3 (Gür et al., 2005, 223 K), SO_2 (Bogumil et al., 2003, 273 K), a Ring spectrum (Bussemer, 1993; Wagner et al., 2009) and an inverse spectrum (both calculated from the direct sun spectrum) are included in the spectral analysis. Also a polynomial of degree 4 is included to

ACPD
10, 29631–29682, 2010

account for broad band effects and atmospheric scattering. Because the atmospheric light paths within the selected fitting window change systematically with wavelength (e.g. van Roozendael et al., 2006), not only the original ozone absorption cross section but also a second one (the original cross section scaled with a fourth order polynomial in wavelength) are included in the fitting algorithm. As the SO_2 column density in this study is rather low, the saturation effects as documented by Richter et al. (2009) or Yang et al. (2009) need not to be considered. The retrieval error of the SO_2 SCD is 5×10^{16} molec cm^{-2}. Hence, it is a factor of ten higher than for CARIBIC DOAS.

The wavelength range from 336 to 360 nm includes 4 BrO bands (Fig. 1 right: O_4 window) and is therefore well suited for the retrieval of the BrO slant column density. The BrO cross section from Wilmouth et al. (1999) was used, the considered ozone cross sections (223 K and 243 K) (Gür et al., 2005) were measured with the flight model spectrometers of GOME-2. Moreover O_4 (Greenblatt et al., 1990), NO_2 (Vandaele et al., 1996), OClO (Bogumil et al., 2003) and SO_2 (Bogumil et al., 2003) were included in the data retrieval. Also in the BrO retrieval a Ring spectrum (Bussemer, 1993; Wagner et al., 2009) and an inverse spectrum were included, calculated from the direct sunlight spectrum. The statistical retrieval error of the BrO SCDs is 3×10^{13} molec cm^{-2}. As a matter of fact, the retrieved column densities in the plume ($\approx6\times10^{13}$ molec cm^{-2}) are close to the detection limit, nevertheless the comparison with the CARIBIC columns shows quite good agreement (Sect. 4.2.2).

In order to calculate the vertical column density in the plume, the measured slant column densities were corrected for the latitudinal and longitudinal dependent offset, which in the case of SO_2 is mainly caused by the spectral interference with ozone or imperfect fitting of the Ring effect. In the case of BrO, the observed volcanic signal is superimposed on the strongly latitudinal-dependent stratospheric BrO distribution. The correction process was only applied to a preselected area of interest (38° W–15° E, 35° N–72° N), including 3 adjacent GOME-2 orbits. To account for the different viewing directions of the individual pixel, the SO_2 and BrO SCDs are converted to VCD by

ACPD
10, 29631–29682, 2010

applying the geometric AMF:

$$\mathrm{AMF}_{\mathrm{geom}} = \frac{1}{\cos(\mathrm{LOS})} + \frac{1}{\cos(\mathrm{SZA})} \quad (5)$$

Here, LOS and SZA are the line of sight (nadir=0°) and the solar zenith angle, respectively. As the $\mathrm{VCD}_{\mathrm{geom}}$ is independent of the LOS, the back-ground can now be estimated as a smooth function of the pixels outside the plume. Therefore, a 2-dimensional polynomial fit of 3rd order was applied to the VCD of all pixels, where the SO_2 VCD does not exceed the 1σ variation (and therefore are supposed not to be part of the volcanic plume).

The corresponding BrO $\mathrm{VCDs}_{\mathrm{geom}}$ were fitted by a 2-dimensional polynomial of 4th order to the same back ground pixels. By subtracting the resulting polynomial from all VCDs (including the VCDs from the presumed volcanic plume pixels) we obtained the offset corrected (normalised) vertical column densities $\mathrm{VCD}_{\mathrm{norm}}$ (Fig. 12).

During the plume observation the SZA was ≈44°, hence the geometrical AMF varied between 2.4 (nadir) and 2.8 (LOS ±45°). For the direct comparison to the CARIBIC DOAS observation (Sect. 4.2) radiative transfer simulations with McArtim (Sect. 2.2) (Deutschmann, 2009) were performed including the same cloud and aerosol settings as for CARIBIC DOAS. Beforehand the corrected $\mathrm{VCD}_{\mathrm{norm}}$ is multiplied with the geometric AMF to calculate a corrected slant column density $\mathrm{SCD}_{\mathrm{norm}}$.

For the retrieval of the BrO vertical column densities the error of slant column densities is dominating and the error of the AMF (Sect. 2.2) can be neglected. Therefore the total error can be estimated by $3\times10^{13}/\mathrm{AMF}\approx1.6\times10^{13}$ molec cm^{-2}. For the SO_2 vertical column densities the error of the AMF is included, which results in a total error of 3.4×10^{16} molec cm^{-2}.

ACPD
10, 29631–29682, 2010

3 Observations

3.1 Measurement flights

Three special measurement flights were performed to help validate the volcanic ash forecasts. Several forecast models (e.g. VAAC, British Met Office (Fig. 3), Eurad (Uni-Köln), Flexpart (NILU)) were compared to get the best possible estimate on the plume's position and movement. Obviously no fly zones as stipulated by the European Volcanic Ash Advisory Centre had to be avoided at all times. According to the forecasts (Fig. 3) for 16 May 2010 the optimal areas to observe particle mass concentrations close to the given aviation safety threshold of 2000 $\mu g\,m^{-3}$ were over Ireland and the Irish Sea and accordingly these areas were probed, with a first leg over Ireland and a second one over the Irish Sea. The transfer flights to and from Ireland were flown at higher altitude (Fig. 4) to reach the research airspace at minimum cost and time.

The actual flight pattern is shown in Fig. 4. As the airspace north of the Isle of Man (≈54° N) was closed, the plane had to turn south at this point. During the plume observation the flight altitude varied between 2 and 7 km. This altitude range was chosen because above flight level 200 (6.1 km) the models predicted low concentrations. On the same day the DLR Falcon also performed measurements over the British Isles and its lidar data observed the maximum plume altitude at 6 km (Schumann et al., 2010) only a few hundred kilometres east over the North Sea close to the British coast (54.6° N, 0.2° W).

The TRAJKS back trajectories (http://www.knmi.nl/samenw/campaign_support/CARIBIC/, September 2010) calculated for various positions along the CARIBIC flight track, indicate that the air masses showing the highest volcanic signals (Sect. 3.2 – north of Ireland) had passed Southern Iceland 58±9 h before the observation (Fig. 5).

ACPD
10, 29631–29682, 2010

3.2 CARIBIC DOAS observation

The DOAS instrument measured three major enhancements of SO_2 (Fig. 6): two of them were very close together (10:05–10:25 LT) and a third, weaker one was measured about 2 h later over the Irish Sea. The first two SO_2 peaks can be attributed to the same plume (Fig. 6). It was observed north of Ireland (Fig. 6) just before and after the u-turn. At the same time enhanced BrO was observed as shown in Figs. 1 and 6.

We are confident that the third peak is just the edge of the large plume that extends further north (Fig. 13), although the Airbus could not fly further north due to the aviation safety rules. At the plume's edge no BrO was observed. Based on the elemental composition of aerosol sample No 6 taken between 11:38:19 and 12:27:20 LT, the minor peak south of the Isle of Man can also be attributed to the volcanic plume (Sect. 3.3.1).

The oxygen dimer O_4 provides a standard tool for passive DOAS observations to estimate the aerosol optical thickness along the light path (e.g. Wagner et al., 2004; Frieß et al., 2006; Heue, 2005). Therefore the observed O_4 slant column densities are compared to calculated SCDs* (Sect. 2.2) based on radiative transfer simulations. The parameterisation of the aerosol extinction in the model is adapted to the measurement. Other parameters e.g. cloud cover, solar zenith angle, and viewing geometry, are included in the model. In Fig. 7 the decrease in the O_4 SCD* and the simultaneous increase in the SO_2 column densities is shown. The coincidence with the SO_2 peaks indicates convincingly that volcanic aerosols caused the observed reductions in the light path.

However, because there was nearly complete cloud cover below the plane, the cloud top height and optical thickness have to be included in the radiative transfer simulation. The video camera in the pylon has an elevation of −13.2°, and a field of view of 36°. When a cloud is first observed in the centre of the video image and a few seconds later at its lower edge, this information can be used to estimate the cloud top height (1500 m±500 m). The low resolution of the video images however limits the accuracy of this method. Nevertheless the results agree well with independent observations

ACPD
10, 29631–29682, 2010

(MODIS – http://ladsweb.nascom.nasa.gov/, August 2010) of the cloud top height, so in the radiative transfer simulation the cloud top height was fixed to 1.5 km. The geometrical and optical thickness (COT) of the cloud were set to 1 km and 10 (Fig. 8), respectively. The horizontal variability in the COT seems to be small (Fig. 8), hence we assumed the same cloud parameters for the plume as well as for the reference.

The geometrical thickness of the plume was assumed to be constant, with plume bottom at 3 and plume top at 6 km altitude (U. Schumann, personal communication, 2010). The aerosol optical thickness and the single scattering albedo were varied in the range from 0.3 km^{-1} to 2.5 km^{-1} and from 0.8 to 0.99, respectively, for the simulation of the optical properties of the volcanic ash cloud. As the algorithm to calculate the exposure time of the spectrometers still had to be optimised, the intensity ratios were weighted by only 10% compared to the O_4 columns. An aerosol extinction of 0.8 km^{-1} combined with a single scattering albedo of 0.95 leads to the best agreement between simulations and observations. Compared to the MODIS observation the total aerosol extinction (TAE≈1) is much higher, which can at least partly be explained with the higher spatial resolution of the CARIBIC DOAS instrument (2 km to 15 km) and by the slight temporal mismatch (10:20 UTC for CARIBIC and 10:56 UTC for MODIS) combined with the strong variability of the volcanic ash cloud.

3.3 Other CARIBIC data

As the aeroplane flew over the ash cloud first and went through it after the u-turn, most instruments observed the plume during the second leg. However, just before the first SO_2 peak a small aerosol peak was detected, perhaps remains of an older plume at higher altitude, or a small streak that reached slightly higher.

3.3.1 Aerosols

During the flight on 16 May 2010 the optical particle counter (Sect. 2.1) failed. Therefore no data about the size distribution in the range from 125 nm to 1 µm inside the

ACPD
10, 29631–29682, 2010

volcanic ash plume were measured. The CPCs (condensation particle counters) measure small particles and cover the size range of 4 nm to 2 µm providing three size bins of 4–12 nm, 12–18 nm and above 18 nm. The respective results are illustrated in Fig. 9. The first aerosol peak seems not to correlate with DOAS O_4 or SO_2 data. This indicates that the condensation nuclei number density is dominated by small particles, which have only a minor influence on the O_4 SCD*. The second and third peak were observed just before the SO_2 column densities peak. In contrast to the third peak the aerosol number concentration of the second one reaches background levels before the DOAS instrument observes the plume's maximum. The aerosol data indicate that the aeroplane passed through the main plume during the period when the second SO_2 peak was observed. Whether or not the first two narrow peaks can be attributed to parts of the plume cannot be inferred from our observation.

Moreover, during the plume observations aerosol samples were collected from 9:59:32 to 10:49:09 LT and 11:38:19 to 12:27:20 LT (Fig. 6). Based on the particle-induced X-ray emission (PIXE) analysis the aerosols were clearly identified as being of volcanic origin by their enhanced concentration of several elements such as silicon, potassium, calcium and iron (samples 4 and 6). We found a similar elemental composition for a volcanic ash sample from Iceland, and Flentje et al. (2010) also reported a similar composition for rain water probes containing washed out particles at Hohenpeißenberg. In addition to these crustal elements, the CARIBIC aerosol samples contained enhanced concentrations of secondarily produced sulphurous aerosol as well as carbonaceous matter, in agreement with observations from the 2008 eruption of the Kasatochi volcano (Martinsson et al., 2009).

3.3.2 Mercury, ozone and carbon monoxide

CARIBIC measures mercury with a single amalgamation, cold vapour atomic fluorescence analyzer (Brenninkmeijer et al., 2007). Volcanoes are known to be a source of atmospheric mercury, but chemical reactions of mercury with volcanic emitted halogens result in some models predicting a decrease of Hg inside a plume (e.g. von

ACPD
10, 29631–29682, 2010

Glasow, 2010). However, in the measured concentrations (Fig. 9) neither an increase nor a decrease is discernible.

The CARIBIC flying laboratory contains two ozone analysers (Brenninkmeijer et al., 2007), namely a fast (0.2 s) chemiluminescence and a slower (4 s) UV absorption instrument. Since the UV absorption instrument is more accurate, its data are shown in Fig. 9. However, it has a weak cross sensitivity to SO_2 caused by the absorption cross section of SO_2 in the UV range. The interference is proportional to the ratio of the absorption cross sections. At 265 nm the ratio $\frac{\sigma(SO_2)}{\sigma(O_3)}$ is close to 4×10^{-2} i.e. an additional SO_2 mixing ratio of 40 ppb (Sect. 4.1) causes an overestimation of 1.6 ppb in O_3. This difference is too small to be resolved by the two ozone analysers.

The ozone mixing ratio is enhanced during the first aerosol peak, indicating that the local air masses might have been stratospherically influenced. During the second observation of the plume, however, it slightly decreases (to 25 ppb), which compared to the background variations is not significant.

During the observation of the second SO_2 peak an increase in CO is observed, while for the first peak again the stratospheric signal (here a decrease) is found. The increase of 70 ppb is not a specific, but in this case clear indicator for the volcanic plume (e.g. Mori and Notsu, 1997). Similar observations (≈60 ppb) are reported by Schumann et al. (2010) for measurements on 17 May 2010.

Several in situ measurements show evidence of volcanic influence during the DOAS observation of the second SO_2 peak. During, or rather prior to the first observation only an increase in the aerosol was found, preceding the SO_2 and O_4 column density increase. The aerosol peak does however correlate with high O_3 values. We conclude that the aeroplane crossed above the plume before it turned around, descended and subsequently crossed the plume.

ACPD
10, 29631–29682, 2010

3.3.3 Hydrocarbons

Volcanoes do not to emit any higher hydrocarbons. On contrary the emitted gases, via complex chemistry, reduce the mixing ratios of a suite of hydrocarbons within the plume. In particular free chlorine radicals formed in the plume deplete a number of hydrocarbons, e.g. ethane and propane (Fig. 10, whole air sample no 9, 10:25 UTC), whereas benzene which has a much slower rate of reaction with chlorine, remained unaffected (Baker et al., 2010b). The fact that the reactive hydrocarbons are not or very little reduced in the preceding samples (7 and 8) until 10:15 UTC confirms that the plane flew over the plume during this period. Samples no 13 to 16 were influenced by marine air masses according to the back trajectories.

3.4 Satellite data

Satellite instruments e.g. OMI (Ozone Monitoring Instrument, Levelt et al., 2006) on AURA and GOME-2 on Metop-A (Sect. 2.3) observed the evolution of Eyjafjallajökull's plume right from the beginning. The SO_2 columns were astonishingly low during the first phase of the eruption until 18 April 2010, thereafter substantial SO_2 column densities were observed.

Figure 11 shows the SO_2 distribution over Western Europe on 16 May 2010. An SO_2 plume appears to be moving from Southern Iceland towards the British Isles, where the remainders of an older plume are located which moved towards Belgium and the Netherlands the following day. The AURA satellite, carrying also the OMI instrument, passed over Europe around noon (12:51 UTC). To minimize time differences the CARIBIC data is compared to the GOME-2 data (Fig. 12) where the maximum difference in the overpass times is less 15 min. In Fig. 12 only the forward scans are considered, in the overlap regions (Sect. 2.3) the averages are shown. The SO_2 data show a compact plume situated over Northern England, with the BrO plume being patchy. The main reason for the high spatial variation in the BrO is likely to be instrumental noise (Sect. 2.3). For both SO_2 and BrO an enhancement is also observed north of

ACPD
10, 29631–29682, 2010

Ireland where the CARIBIC flying laboratory observed the plume (6.67° W/56.07° N).

4 Discussion

4.1 CARIBIC DOAS data

Both viewing directions of the DOAS instrument observed the plume twice with the horizontal distance between the two observations being approximately 15 km. Especially in the −10°, line of sight the differences between the SO_2 slant column densities are quite obvious (Figs. 6 and 13). However, despite some variations of the SO_2 concentrations inside the plume also the different sensitivity for the SO_2 layer, caused by the change in flight altitude is very important for the understanding of the SCDs.

The AMF for SO_2 (315 nm – Fig. 14) and BrO (340 nm) were simulated using the aerosol properties as retrieved from the O_4 column densities (Sect. 3.2). Inside the plume the visibility is strongly reduced by the volcanic aerosol, therefore the Box AMFs decrease very fast with distance from the plane.

The SO_2 vertical column densities (Eqs. 3 and 4) for −10°, and nadir agree quite well (Fig. 15), with only the first observation of the plume with the −10°, telescope being slightly smaller than the respective nadir observation. This might be caused by some local variations in the SO_2 concentration, both horizontally and vertically. For BrO this effect is smaller, however as the noise in the −10°, data is high, we assume the relative distributions of BrO and SO_2 to be the same. Because the viewing direction changed rapidly during the turn no AMFs are calculated for this flight section.

In contrast to other observations made close to a volcanic crater (e.g. Bobrowski et al., 2007), we observe no increase in the BrO to SO_2 ratio towards the edges. This was to be expected as the O_3 mixing ratio in the plume centre (Fig. 9 ≈25 to 50 ppb) is still high enough for the oxidation of bromine (R5). According to von Glasow (2010) between 10 and 30% of the total bromine in the plume is BrO, the retrieved BrO mixing ratio (Table 2) of 5 ppt therefore results in a total bromine content of 15 to 50 ppt, which

ACPD
10, 29631–29682, 2010

is still much lower than the observed ozone mixing ratio of 25–50 ppb.

If we assume a constant mixing ratio for the complete layer from 3 to 6 km we retrieve roughly 40 ppb for SO_2 and 5 ppt BrO (Table 2). The values in Table 2 are calculated with the maximum observations of the 80 s averages, the individual 8 s spectra result in similar mixing ratios with a 1-σ variation of 1.8 ppt BrO and 1.2 ppb SO_2 during the observation of the maximum in the nadir data. A better agreement between the vertical columns or the mixing ratios of the four individual observations cannot be expected, since different air masses were observed. The difference of 10 min corresponds to 6 km shift of the plume according to the wind speed (20 knts $\approx 10\,m\,s^{-1}$), which is not enough to compensate for the difference of 15 km between the two observation points. In situ SO_2 measurements on the DLR Falcon over the British east coast reached values over 30 ppb on the same day but a few hours later (Schumann et al., 2010). This is in good agreement with our data; although a different part of the plume was probed.

The horizontal extension of the plume is estimated based on the width of the SO_2 peaks. The fact that two peaks can be distinguished in the time series of the SO_2 and the BrO column densities proofs that for the short period in between the aeroplane did neither sample inside the plume nor flew over it. If this short period was due to the fact that the aeroplane briefly left the plume to return later, we calculate that the plume was 60 km wide. Compared to the model prediction (Fig. 3) the observed SO_2 plume is further north and smaller. The fact that the O_4 time series (Fig. 7) show a similar pattern indicates that the SO_2 and the aerosol plume coincide.

4.2 Comparison with GOME-2 satellite data

Comparing airborne DOAS observations with those from satellites always faces two questions:

– What influence has the spatial distribution of the trace gases on the columns observed by the two instruments with different resolution?

ACPD
10, 29631–29682, 2010

– If the spatial variation is small enough, do the instruments agree when the same air masses are observed?

Based on previous comparisons (Heue et al., 2010) we know that both observations can agree very well if the AMFs are calculated using the correct cloud and aerosol description and the data are corrected for differences in overpass times. In this study the measurements were almost simultaneously i.e. 10:05 to 10:25 UTC for CARIBIC and 10:09 for GOME-2. Therefore large parts of the observed differences are most probably caused by the different spatial resolution of the two instruments in combination with the distribution of the trace gases.

4.2.1 Sulphur dioxide vertical column densities

A comparison of the SO_2 vertical columns is shown in Fig. 16, the surrounding GOME-2 pixels are shown for each CARIBIC DOAS observation, including forward and backward scan, as well as overlapping pixels. The lengths of the GOME-2 measurement points in this "time series" are given by the time the CARIBIC system spent in the respective pixel. The figure shows a clear symmetry for GOME-2, which is caused by the fact that before, and after the u-turn CARIBIC flew over the same GOME-2 pixels.

The location of the SO_2 maximum agrees well with the CARIBIC observation for both forward and back scan. Also the minimum to the north of the plume (10:15 UTC-CARIBIC) can be seen in the GOME-2 dataset. Due to the smaller pixel size the maxima are more pronounced in the forward scan, compared to the back scan, where additional parts of the plume might be observed further east and west. Therefore it is apparently surprising that the better quantitative agreement with respect to the vertical column density is found for the backward scan. This finding can be understood when taking into account the local distribution of the SO_2 relative to the GOME-2 pixels.

According to Fig. 12, the SO_2 plume is almost parallel to the GOME-2 scan direction. If the plume is located in the centre of the back scan, and extends parallel to the pixel orientation, this might explain why the large back scan observes a higher column

ACPD
10, 29631–29682, 2010

density than the smaller forward scan. At least at the position of the CARIBIC observation the plume was located in the centre of the back scan (Fig. 17). An alternative explanation for higher back scan columns would be that the maximum is further east or west i.e. there is a second SO_2 maximum covered by the back scan but not observed by the respective GOME-2 forward scan. That implies that it is observed by any other forward scan overlapping with this back scan.

The vertical column density for the back scan (swath 27) is 1.49×10^{17} molec cm^{-2}, the VCDs for the respective forward scans are listed in Table 3. Only pixel 19 of swath 28 (not shown in Fig. 2) has a VCD that is higher than the backward scan, due to its small overlap ($\approx$390 km^2) it contributes less than 4% to the back scan VCD.

80% of the area of the forward pixel 21 (swath 27) is also covered by the back scan, therefore the contribution of the back scan signal to this forward scan can easily be estimated. If the plume was homogenously distributed inside the back scan, then the signal of this forward pixel would be higher than 1.2×10^{17} molec cm^{-2}, even if the VCD vanished in the other 20% of the pixel. Therefore the SO_2 column density cannot have been homogenously distributed in the back scan. Of course this was not to be expected, especially as the CARIBIC data already showed local variability.

A combination of the CARIBIC and GOME-2 data might be used to estimate the size of the part of the plume which was observed by CARIBIC. The plume is about 60 km wide (Fig. 17) and the distance between the two CARIBIC observations is about 15 km. If we assume this part of the plume to be 60×40 km^2 with an average VCD of 2×10^{17} molec cm^{-2} (Fig. 16) then it contributes about 98% to the column density observed by GOME-2 forward scan (pixel 21 of swath 27), and 49% to the VCD of the pixel 21 of swath 28. The assumption that the plume expands over 80 km i.e. that it stretches over the complete pixel results in a VCD of 1.7×10^{17} molec cm^{-2} and hence contradicts the observed VCD for pixel 21, swath 27. The same assumption however might explain about 98% of the observed VCD of the same pixel in the next swath (28). The plume was weighted with 75% and 50% as it is not completely covered by the pixel 21 of swath 27 and 28, respectively.

ACPD
10, 29631–29682, 2010

Hence the local variability of the SO_2 concentration or vertical column density must have been higher than expected from CARIBIC and the GOME-2 observations. In this estimate we assumed that outside the plume the vertical column vanishes, but even with this simple approximation we partly overestimated the GOME-2 signal.

To conclude, the plume we observed here with CARIBIC and GOME-2 was about 60 km wide, for the northern GOME-2 pixel (21 swath 27) the length inside the pixel was roughly 30 km or slightly more. For the southern pixel (21 swath 28) the estimated length is close to 80 km (covering the entire length of the pixel). Hence locally the plume did not extend parallel to the GOME-2 pixels but turns south. The shift according to the wind and time is insignificant, since 12 km to the west (20 min) is not enough to transport the observed part of the plume to a different GOME-2 pixel (Fig. 17).

4.2.2 Bromine monoxide vertical column densities

In the CARIBIC DOAS observations SO_2 and BrO do coincide (Fig. 6), indicating that the position of the maxima in the plume are the same. In contrast the BrO maxima in the GOME-2 data are shifted north compared to SO_2 (Fig. 12). Despite this spatial shift in the GOME-2 BrO data, the BrO VCDs of CARIBIC and GOME-2 agree quite well (Fig. 18). Compared to SO_2 (Fig. 16) both data sets are noisier, therefore a detailed study of the local distribution including forward and back scan as well as CARIBIC data cannot be accurate. Nevertheless one interesting case shall be mentioned: at the southern edge of the plume (10:08 and 10:24 UTC) the forward scan observes the background level, whereas the overlapping back scan agrees quite well with maximum of the CARIBIC DOAS measurement. But this agreement is likely caused by higher BrO values observed further east (Fig. 12, at 5° W, over the British coast).

ACPD
10, 29631–29682, 2010

5 Conclusions

The Eyjafjallajökull plume was observed by several instruments of the CARIBIC flying observatory during the special volcanic mission flight on 16 May 2010. While the remote sensing DOAS instrument observed the plume twice north of Ireland, many in situ instruments observed the plume only in the second case. This shows that the aeroplane first flew over the plume, turned around to subsequently cross it. Moreover, it highlights the importance of the remote sensing aspect of the DOAS instrument as a part of CARIBIC. A lot of additional information from the aerosol counters, the ozone and carbon oxide instruments as well as the air samplers is used to determine whether or not the plane was inside the plume, which is essential for the description of the atmosphere during the AMF calculation. Unfortunately the optical particle counter failed during this flight, which might have given very useful additional information on the aerosol optical properties. Chemical evidence that the observed plume originated from the Eyjafjallajökull volcano was given by comparing elemental composition of collected aerosol samples with that of volcanic ash from Iceland. The video camera was for the first time in the CARIBIC project used to give a rough approximation of the cloud top height, which is however limited by the coarse resolution of the video images.

Based on the O_4 column density, the aerosol extinction and single scattering albedo were retrieved. Compared to MODIS satellite data, the retrieved total aerosol optical depth is higher by a factor of 2. The retrieved information was used to calculate the local SO_2 and BrO mixing ratios inside the plume to 40 ppb (29–49) and 5 ppt (4.3–6.0), respectively. The SO_2 mixing ratio agrees well with in situ observation from the DLR Falcon further east. As additional instrument on CARIBIC a SO_2 in situ analyser might be very useful, not only for special missions of volcanic plume hunting. For the small part of the plume sampled during this flight, the MetOffice dispersion model predicted the plume further south and wider than it actually was.

A good agreement is observed between GOME-2 and CARIBIC DOAS for the sulphur dioxide vertical columns, if the cloud altitude and the aerosol extinction in the

ACPD
10, 29631–29682, 2010

plume are considered in the AMF calculation. The GOME-2 BrO columns are close to the detection limit, however, a reasonable agreement could be observed here as well. A more detailed study on the column densities observed by the GOME-2 forward scan and the back scan showed that the local variability of SO_2 concentration is very high. By combining the CARIBIC and the GOME-2 vertical columns we estimated that the observed part plume was 60 km wide and did not cover the entire length (80 km) of the GOME-2 pixels. While the length of the plume in the northern pixel was roughly 30 to 40 km, in the southern part the length almost reached the length of the whole pixel.

Acknowledgements. For providing the MODIS data at http://ladsweb.nascom.nasa.gov/ the MODIS team is acknowledged. We thank the OMI team for providing the figure at: http://www.temis.nl. The volcanic ash forecast groups especially at MetOffice are acknowledged for the forecasts used during flight preparation. Also Ulrich Schumann and the DLR Falcon scientific group are acknowledged for sharing some experiences and preliminary results. We thank Lufthansa Airlines for giving us the opportunity to measure under these unique conditions especially Captain Martin Hoell, Andreas Waibel, Thomas Dauer, Sven Dankert and Detlev Hartwig and of course the CARIBIC Team for their commitment and support. The DOAS system was built and operated by the Institut für Umweltphysik of the Universität Heidelberg. Rinus Scheele (KNMI) is acknowledged for helping with the trajectory calculations. The development and operation of the CARIBIC system has been financially supported by the German Bundesministerium für Bildung und Forschung (BMBF – AFO 2000), by the European Commission's DGXII Environment RTD 4th, 5th and 6th framework programs, by the Max-Planck-Society, EON-Ruhrgas and Frankfurt Airport.

The service charges for this open access publication have been covered by the Max-Planck-Society.

ACPD

10, 29631–29682, 2010

References

Ansmann, A., Tesche, M., Groß, S., Freudenthaler, V., Seifert, P., Hiebsch, A., Schmidt, J., Wandinger, U., Mattis, I., Müller, D., and Wiegner, M.: The 16 April 2010 major volcanic ash plume over Central Europe: EARLINET lidar and AERONET photometer observations at Leipzig and Munich, Germany, Geophys. Res. Lett., 37, L13810, doi:10.1029/2010GL043809, 2010. 29633, 29634

Baker, A. K., Schuck, T. J., Slemr, F., van Velthoven, P., Zahn, A., and Brenninkmeijer, C. A. M.: Characterization of non-methane hydrocarbons in Asian summer monsoon outflow observed by the CARIBIC aircraft, Atmos. Chem. Phys. Discuss., 10, 18101–18138, doi:10.5194/acpd-10-18101-2010, 2010a. 29636

Baker, A. K., Rauthe-Schöch, A., Schuck, T. J., Brenninkmeijer, C. A. M., van Velthoven, P. F. J., and Oram D. E.: Chlorine radical chemistry in the Eyjafjallajökull volcanic plume, in preparation, 2010b. 29649

Bobrowski, N., Hönninger, G., Galle, B., and Platt, U.: Detection of bromine monoxide in a volcanic plume, Nature, 423, 273–276, doi:10.1038/nature01625, 2003. 29634

Bobrowski, N., von Glasow, R., Aiuppa, A., Inguaggiato, S., Louban, I., Ibrahim, O. W., and Platt, U.: Reactive halogen chemistry in volcanic plumes, J. Geophys. Res., 112, D06311, doi:10.1029/2006JD007206, 2007. 29635, 29640, 29650

Bogumil, K., Orphal, J., Homann, T., Voigt, S., Spietz, P., Fleischmann, O. C., Vogel, A., Hartmann, M., Bovensmann, H., Frerik, J., and Burrows, J. P.: Measurements of molecular absorption spectra with the SCIAMACHY pre-flight model: instrument characterization and reference data for atmospheric remote-sensing in the 230–2380 nm region, J. Photoch. Photobio. A, 157, 167–184, doi:10.1016/s1010-6030(03)00062-5, 2003. 29639, 29641, 29642

Brenninkmeijer, C. A. M., Crutzen, P., Boumard, F., Dauer, T., Dix, B., Ebinghaus, R., Filippi, D., Fischer, H., Franke, H., Frieß, U., Heintzenberg, J., Helleis, F., Hermann, M., Kock, H. H., Koeppel, C., Lelieveld, J., Leuenberger, M., Martinsson, B. G., Miemczyk, S., Moret, H. P., Nguyen, H. N., Nyfeler, P., Oram, D., O'Sullivan, D., Penkett, S., Platt, U., Pupek, M., Ramonet, M., Randa, B., Reichelt, M., Rhee, T. S., Rohwer, J., Rosenfeld, K., Scharffe, D., Schlager, H., Schumann, U., Slemr, F., Sprung, D., Stock, P., Thaler, R., Valentino, F., van Velthoven, P., Waibel, A., Wandel, A., Waschitschek, K., Wiedensohler, A., Xueref-Remy, I., Zahn, A., Zech, U., and Ziereis, H.: Civil Aircraft for the regular investigation of the atmosphere based on an instrumented container: The new CARIBIC system, Atmos. Chem.

ACPD
10, 29631–29682, 2010

Phys., 7, 4953–4976, doi:10.5194/acp-7-4953-2007, 2007. 29634, 29647, 29648
Bussemer, M.: Der Ring-Effekt: Ursachen und Einfluß auf die Messung stratosphärischer Spurenstoffe, diploma thesis, University of Heidelberg, Germany, 1993. 29640, 29641, 29642
Carn, S. A., Krueger, A. J., Krotkov, N. A., Yang, K., and Evans, K.: Tracking volcanic sulfur dioxide clouds for aviation hazard mitigation, Nat. Hazards, 51, 325–343, doi:10.1007/s11069-008-9228-4, 2009. 29634
Deutschmann, T.: Atmospheric Radiative Transfer Modelling with Monte Carlo Methods, diploma thesis, University of Heidelberg, Germany, 2009. 29638, 29643
Dix, B., Brenninkmeijer, C. A. M., Frieß, U., Wagner, T., and Platt, U.: Airborne multi-axis DOAS measurements of atmospheric trace gases on CARIBIC long-distance flights, Atmos. Meas. Tech., 2, 639–652, doi:10.5194/amt-2-639-2009, 2009. 29637
Dyroff, C., Fütterer, D., and Zahn, A.: Compact diode-laser spectrometer ISOWAT for highly sensitive airborne measurements of water-isotope ratios, Appl. Phys. B-Lasers O., 98(2–3), 537–548, doi:10.1007/s00340-009-3775-6, 2010. 29636
Flentje, H., Claude, H., Elste, T., Gilge, S., Köhler, U., Plass-Dülmer, C., Steinbrecht, W., Thomas, W., Werner, A., and Fricke, W.: The Eyjafjallajökull eruption in April 2010 – detection of volcanic plume using in-situ measurements, ozone sondes and lidar-ceilometer profiles, Atmos. Chem. Phys., 10, 10085–10092, doi:10.5194/acp-10-10085-2010, 2010. 29634, 29647
Frieß, U., Monks, P. S., Remedios, J. J., Rozanov, A., Sinreich, R., Wagner, T., and Platt, U.: MAX-DOAS O_4 measurements: a new technique to derive information on atmospheric aerosols: 2. Modelling studies, J. Geophys. Res., 111, D14203, doi:10.1029/2005JD006618, 2006. 29645
von Glasow, R.: Atmospheric chemistry in volcanic plumes, P. Natl. Acad. Sci. USA, 107, 15, 6594–6599, doi:10.1073/pnas.0913164107, 2010. 29647, 29650
von Glasow, R., Bobrowski, N., and Kern, C.: The effects of volcanic eruptions on atmospheric chemistry, Chem. Geol., 263, 131–142, doi:10.1016/j.chemgeo.2008.08.020, 2009. 29634
Grainger, J. and Ring, J.: Anomalous Fraunhofer line profiles, Nature, 193, 762, 1962. 29640
Greenblatt, G. D., Orlando, J. J., Burkholder, J. B., and Ravishankara, A. R.: Absorption measurements of oxygen between 330 and 1140 nm, J. Geophys. Res., 95, 18577–18582, 1990. 29639, 29642
Gür, B., Spietz, P., Orphal, J., and Burrows, J.: Absorption Spectra Measurements with the

ACPD
10, 29631–29682, 2010

GOME-2 FMs using the IUP/IFE-UBs Calibration Apparatus for Trace Gas Absorption Spectroscopy CATGAS, Final Report, IUP University of Bremen, 2005. 29641, 29642
Heue, K.-P.: Airborne Multi AXes DOAS Instrument and Measurements of Two Dimensional Trace Gas Distribution, Ph.D. thesis, University of Heidelberg, Germany, 2005. 29645
Heue, K.-P., Brenninkmeijer, C. A. M., Wagner, T., Mies, K., Dix, B., Frieß, U., Martinsson, B. G., Slemr, F., and van Velthoven, P. F. J.: Observations of the 2008 Kasatochi volcanic SO_2 plume by CARIBIC aircraft DOAS and the GOME-2 satellite, Atmos. Chem. Phys., 10, 4699–4713, doi:10.5194/acp-10-4699-2010, 2010. 29637, 29638, 29641, 29652
Kattner, L., Dyroff, C., and Zahn, A.: An ICOS laser spectrometer for regular in-situ measurements of CH_4 and CO_2 aboard the CARIBIC passenger aircraft, Poster presentation at EGU general Assembly, Vienna, 2–7 May 2010, EGU2010-9997, 2010. 29636
Kraus, S.: DOASIS – a FramewoKraus, S.: DOASIS – A framework Design for DOAS, Dissertation, University of Mannheim, Germany, 2005. 29640
Kromminga, H., Orphal, J., Spietz, P., Voigt, S. and Burrows, J. P.: New measurements of OClO absorption cross sections in the 325–435 nm and their temperature dependence between 213–293 K, J. Photochem. Photobiol. C, 157, 149–160, doi:10.1016/s1010-6030(03)00071-6, 2003. 29640
Levelt, P. F., van den Oord, G. H. J., Dobber, M. R., Mälkki, A., Visser, H., de Vries, J., Stammes, P., Lundell, J., and Saari, H.: The ozone monitoring instrument, IEEE T. Geosci. Remote, 44, 5, 1093–1101, doi:10.1109/TGRS.2006.872333, 2006. 29649
Martinsson, B. G., Brenninkmeijer, C. A. M., Carn, S. A., Hermann, M., Heue, K.-P., van Velthoven, P. F. J., and Zahn, A.: Influence of the 2008 Kasatochi volcanic eruption on sulfurous and carbonaceous aerosol constituents in the lower stratosphere, Geophys. Res. Lett., 36, L12813, doi:10.1029/2009GL038735, 2009. 29647
Mori, T. and Notsu, K.: Remote CO, COS, CO_2, SO_2, HC1 detection and temperature estimation of volcanic gas, Geophys. Res. Lett., 24, 2047–2050, 0094-8534/97/97GL-52058505.00, 1997. 29648
Nguyen, H. N., Gudmundsson, A., and Martinsson, B. G.: Design and calibration of a multichannel aerosol sampler for tropopause region studies from the CARIBIC platform, Aerosol Sci. Tech., 40, 649–655, doi:10.1080/02786820600767807, 2006. 29636
Platt, U. and Stutz, J.: Differential Optical Absorption Spectroscopy, Principles and Applications, Springer, Berlin Heidelberg, 2008. 29637
Richter, A., Wittrock, F., Schönhardt, A., and Burrows, J. P.: Quantifying volcanic SO_2 emis-

ACPD
10, 29631–29682, 2010

sions using GOME-2 measurements, Poster presentation at EGU General Assembly, Vienna, Austria, 19–24 April 2009, AS3.15 XY247, available at: http://www.iup.uni-bremen.de/doas/posters/egu_2009_richter.pdf, last access: 11 January 2010, 2009. 29642

van Roozendael, M., Loyola, D., Spurr, R., Balis, D., Lambert, J.-C., Livschitz, Y., Valks, P., Ruppert, T., Kenter, P., Fayt, C., and Zehner, C.: Ten years of GOME/ERS-2 total ozone data – the new GOME data processor (GDP) version 4: 1. Algorithm description, J. Geophys. Res., 111, D14311, doi:10.1029/2005JD006375, 2006. 29642

Sander, R., Vogt, R., Harris, G. W., and Crutzen, P. J.: Modeling the chemitry of ozone, halogen compounds and hydrocarbons in the arctic troposphere during spring, Tellus, 49B(5), 522–532, 1997. 29635

Scheele, M. P., Siegmund, P. C., and van Velthoven, P. F. J.: Sensitivity of trajectories to data resolution and its dependence on the starting point: in or outside a tropopause fold, Meteorol. Appl., 3, 267–273, 1996. 29636

Schuck, T. J., Brenninkmeijer, C. A. M., Slemr, F., Xueref-Remy, I., and Zahn, A.: Greenhouse gas analysis of air samples collected onboard the CARIBIC passenger aircraft, Atmos. Meas. Tech., 2, 449–464, doi:10.5194/amt-2-449-2009, 2009. 29636

Schumann, U., Weinzierl, B., Reitebuch, O., Schlager, H., Minikin, A., Forster, C., Baumann, R., Sailer, T., Graf, K., Mannstein, H., Voigt, C., Rahm, S., Simmet, R., Scheibe, M., Lichtenstern, M., Stock, P., Rüba, H., Schäuble, D., Tafferner, A., Rautenhaus, M., Gerz, T., Ziereis, H., Krautstrunk, M., Mallaun, C., Gayet, J.-F., Lieke, K., Kandler, K., Ebert, M., Weinbruch, S., Stohl, A., Gasteiger, J., Olafsson, H., and Sturm, K.: Airborne observations of the Eyjafjalla volcano ash cloud over Europe during air space closure in April and May 2010, Atmos. Chem. Phys. Discuss., 10, 22131–22218, doi:10.5194/acpd-10-22131-2010, 2010. 29633, 29634, 29644, 29648, 29651

Simpson, W. R., von Glasow, R., Riedel, K., Anderson, P., Ariya, P., Bottenheim, J., Burrows, J., Carpenter, L. J., Frieß, U., Goodsite, M. E., Heard, D., Hutterli, M., Jacobi, H.-W., Kaleschke, L., Neff, B., Plane, J., Platt, U., Richter, A., Roscoe, H., Sander, R., Shepson, P., Sodeau, J., Steffen, A., Wagner, T., and Wolff, E.: Halogens and their role in polar boundary-layer ozone depletion, Atmos. Chem. Phys., 7, 4375–4418, doi:10.5194/acp-7-4375-2007, 2007. 29635

Stohl, A., Haimberger, L., Scheele, M. P., and Wernli, H.: An intercomparison of results from three trajectory models, Meteorol. Appl., 8, 127–135, 2001. 29636

Vandaele, A. C., Hermans, C., Simon, P., C., van Roozendael, M., Guilmot, J. M., Carleer, M.,

ACPD
10, 29631–29682, 2010

and Colin, R.: Fourier transform measurement of NO_2 absorption cross section in the visible range at room temperature, J. Atmos. Chem., 25(3), 289–305, 1996. 29639, 29642

Wagner, T., Dix, B., von Friedeburg, C., Frieß, U., Sanghavi, S., Sinreich, R., and Platt, U.: MAX-DOAS O_4 measurements: a new technique to derive information on atmospheric aerosols – principles and information content, J. Geophys. Res., 109, D22205, doi:10.1029/2004JD004904, 2004. 29645

Wagner, T., Beirle, S., and Deutschmann, T.: Three-dimensional simulation of the Ring effect in observations of scattered sun light using Monte Carlo radiative transfer models, Atmos. Meas. Tech., 2, 113–124, doi:10.5194/amt-2-113-2009, 2009. 29641, 29642

Wilmouth, D. M., Hanisco, T. F., Donahue, N. M., and Anderson, J. G.: Fourier transform ultraviolet spectroscopy of the A 2Π3/2←X 2Π3/2 transition of BrO, J. Phys. Chem. A, 103, 8935–8945, 1999. 29639, 29642

Yang, K., Krotkov, N. A., Krueger, A. J., Carn, S. A., Bhartia, P. K., and Levelt, P. F.: Improving retrieval of volcanic sulfur dioxide from backscattered UV satellite observations, Geophys. Res. Lett., 36, L03102, doi:10.1029/2008GL036036, 2009. 29642

ACPD

10, 29631–29682, 2010

Table 1. Error estimates for BrO and SO_2 vertical column densities for the two lines of sight during the observation of the plume (Sect. 4.1).

	BrO [10^{13} molec cm^{-2}]	SO_2 [10^{16} molec cm^{-2}]
−10°	1.8	1.9
nadir	0.8	1.8

ACPD
10, 29631–29682, 2010

Table 2. Overview of the retrieved BrO and SO_2 mixing ratios based on the CARIBIC DOAS data for the four individual observations of the plume. The variability in the SO_2 data is quite high, which might be caused by the local distribution. Even if the BrO mixing ratio is constant, the error (1.8 ppt) is too high to assume that the distribution differs from the SO_2 distribution.

	BrO [ppt]		SO_2 [ppb]		$\frac{BrO}{SO_2}$ [10^{-4}]	
	−10°	Nadir	−10°	Nadir	−10°	Nadir
1st peak	4.9	4.3	29.3	35.3	1.69	1.22
2nd peak	6.0	4.5	49.7	45.7	1.21	0.98

ACPD
10, 29631–29682, 2010

Table 3. Vertical SO_2 column densities in 10^{17} molec cm^{-2} for the GOME-2 forward scan pixels overlapping with that back scan, where the maximum of 1.49×10^{17} molec cm^{-2} in SO_2 is observed (in red). In black are those pixels that are also probed by CARIBIC and in grey are the neighbouring pixels.

SwathNo/PixelNo	19	20	21	22	28 back scan, swath 27
27	1.12	1.25	0.86	0.37	1.49
28	1.86	1.28	1.14	1.43	

ACPD
10, 29631–29682, 2010

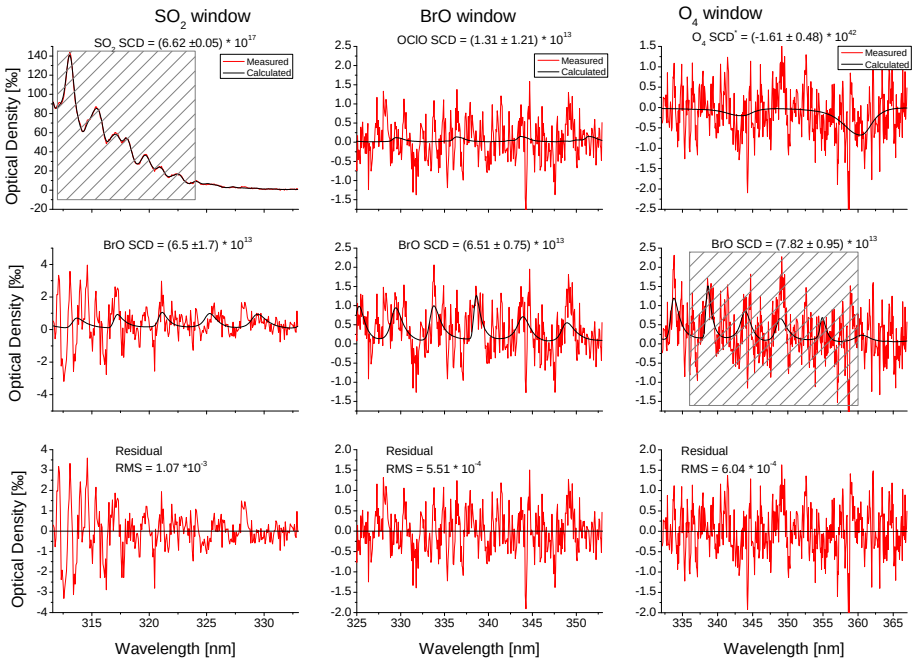

Fig. 1. Example fit for the three different wavelength intervals for spectrum C4000160 (9 spectra co-added 10:19:28–10:20:50 UTC) of the nadir spectrometer (6.66° W, 56.14° N, 4580 m a.s.l. – inside the plume). The hatched areas in the SO_2 and O_4 windows show the SO_2 and BrO fit window used in the GOME-2 retrieval (Sect. 2.3).

ACPD
10, 29631–29682, 2010

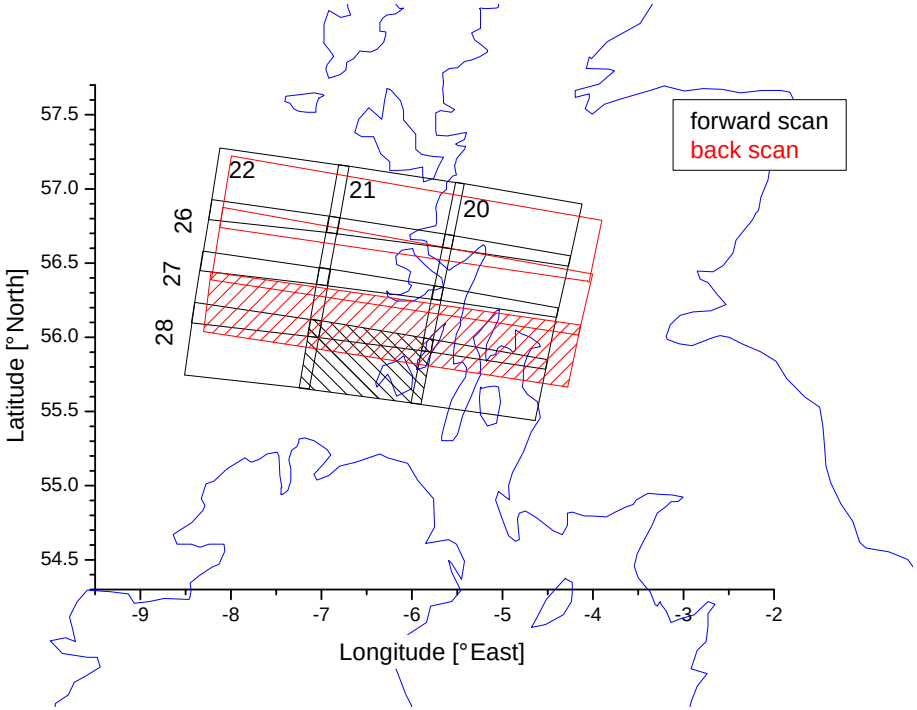

Fig. 2. Forward (black) and back scans (red) of the GOME-2 instrument north of Ireland (16 May 2010 10:09 UTC). For both scanning modes one pixel is hatched to emphasise the size of the individual pixels and to illustrate the overlapping areas. The numbers in the forward pixels indicate the pixel number, while the swatch number is written to the left.

ACPD
10, 29631–29682, 2010

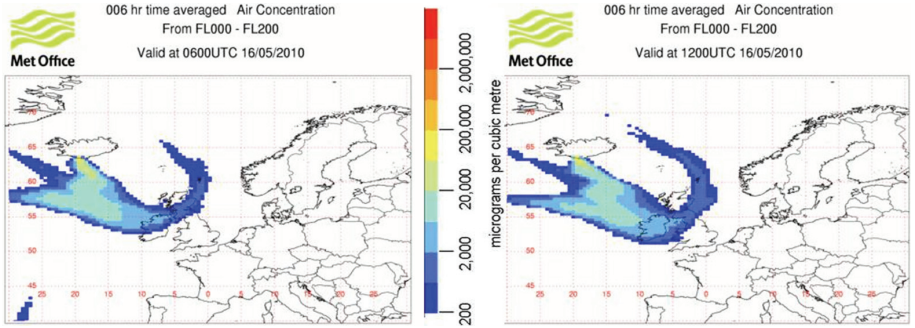

Fig. 3. The volcanic ash forecast from the British Met Office for 16 May 2010, 6:00 UTC (left) and 12:00 UTC (right) for the flight levels 0 to 200 (surface to 6.1 km). The centre of the plume was expected to be south of Iceland and expanding over Ireland with a small filament reaching from Northern England almost back to Iceland. Comparing the two panels shows that the plume was expected to move south-west.

ACPD
10, 29631–29682, 2010

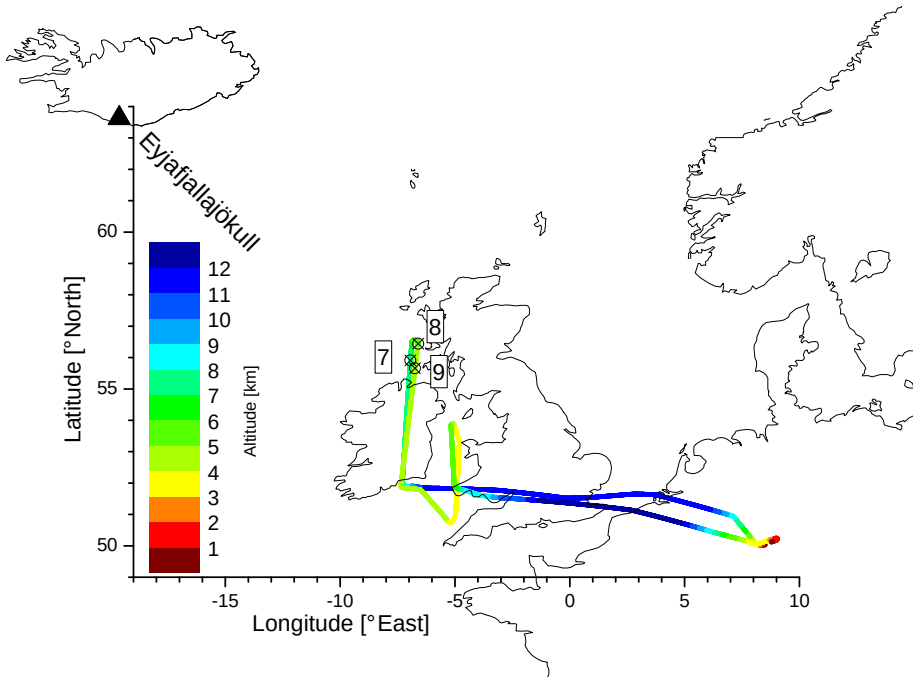

Fig. 4. Flight track of the Lufthansa Airbus during the special CARIBIC mission on 16 May 2010. The flight pressure altitude is colour coded, low altitudes in red. The position of the air samples 7, 8 and 9 are labelled by their respective number (Fig. 10). Close to the Isle of Man the plane had to turn south as the airspace further north (≈54° N) was being closed by the time the plane reached that point.

ACPD
10, 29631–29682, 2010

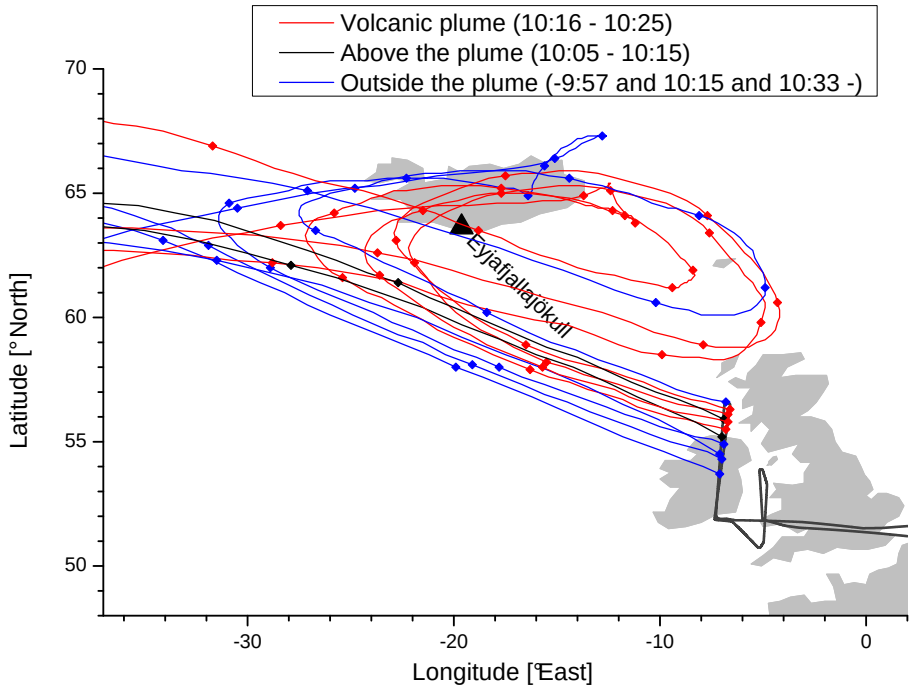

Fig. 5. TRAJKS backward trajectories, for the time of the CARIBIC plume observation. The dots along the trajectories label 12 h intervals. With the DOAS the plume was observed twice, as the aeroplane crossed over the plume and subsequently descended to plume altitude (Sects. 3.2 and 3.3). The trajectories for the period during which many other instruments showed influence of volcanic air masses are illustrated in red, the blue lines show clean air, and the black lines stand for the periods of enhanced DOAS SO_2 signal without additional indicators for volcanic influences. The origin of the enhanced SO_2 values can be traced back to the Eyjafjallajökull volcano on Iceland, which the air masses had passed 58±9 h before the CARIBIC sampled the plume (16 May 2010 10:20 UTC).

ACPD
10, 29631–29682, 2010

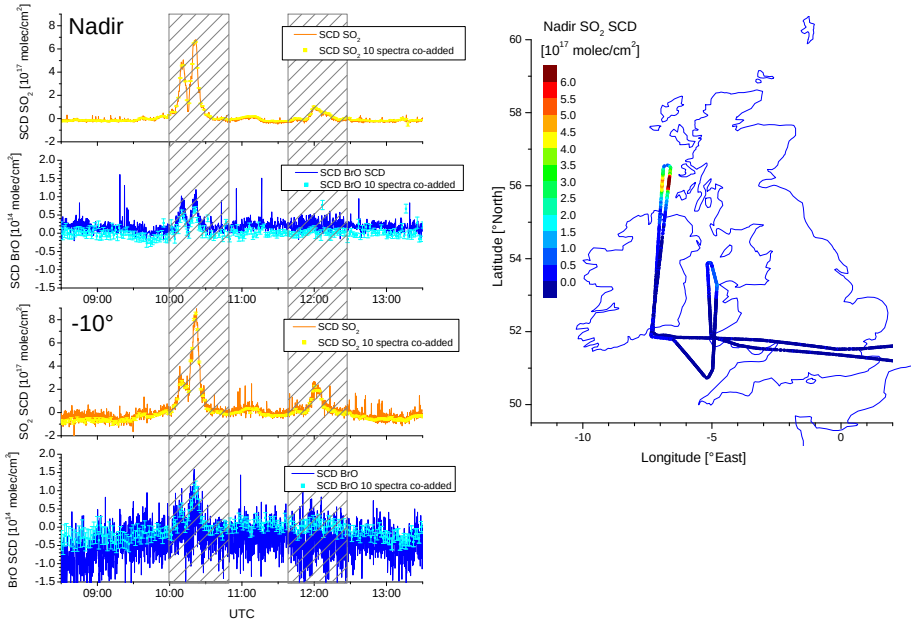

Fig. 6. Time series of the SO_2 and the BrO CARIBIC DOAS SCDs for nadir and −10° and the spatial SO_2 distribution (right) for nadir. The two strong enhancements can clearly be attributed to the same plume which was crossed twice just before and after the u-turn north of Ireland. The hatched areas indicate the two time intervals during which the collected aerosol samples showed clear evidence of volcanic ash.

ACPD
10, 29631–29682, 2010

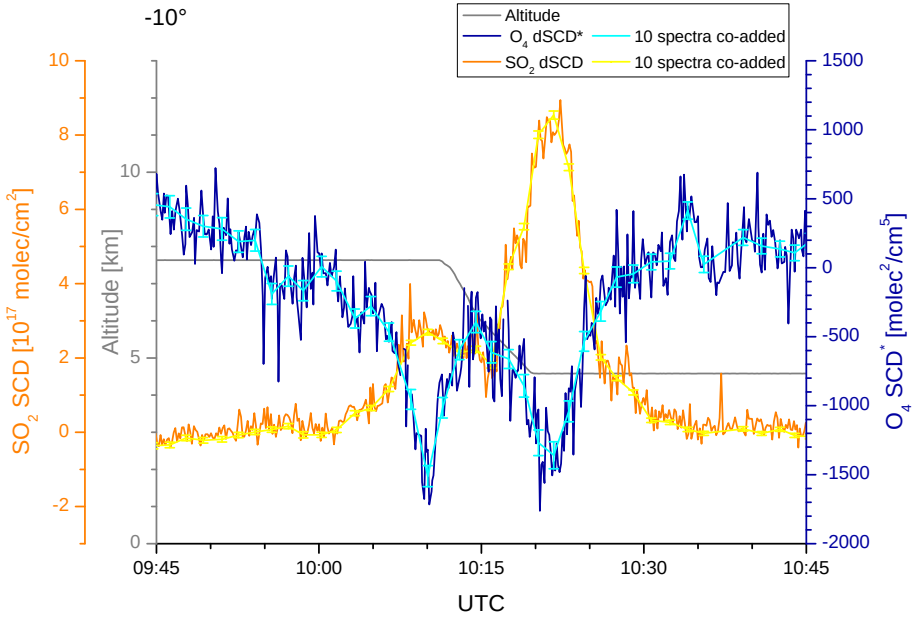

Fig. 7. CARIBIC DOAS O_4 SCD* of the −10° telescope and the flight altitude during the observation of enhanced SO_2 column densities. Due to the volcanic ash the light path through and in the plume is strongly reduced, resulting in lower O_4 slant column densities.

ACPD
10, 29631–29682, 2010

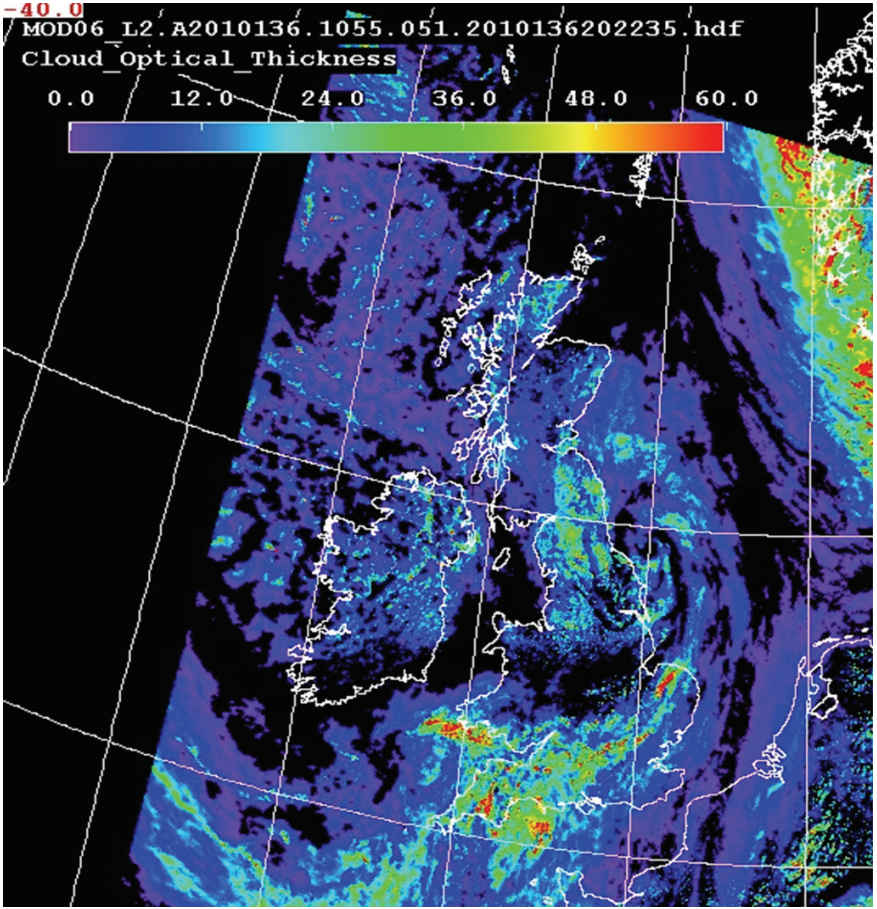

Fig. 8. MODIS cloud optical thickness over the British Isles for 16 May 2010. North of Ireland the COT was around 10 with very small variations.

ACPD
10, 29631–29682, 2010

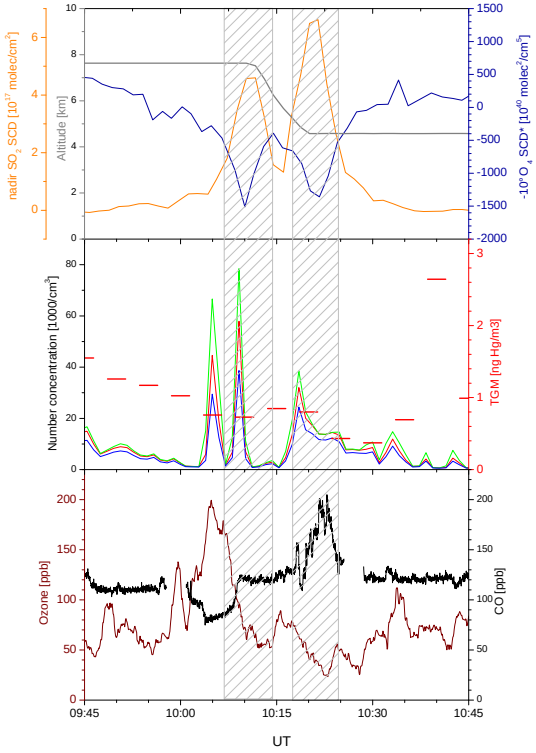

Fig. 9. Overview of additional CARIBIC observations and the DOAS SO_2 and O_4 data (Fig. 7). Three increases in the aerosol number concentrations occurred. The green, red and blue line corresponds to the size bin above 4 mm, above 12 mm and above 18 mm, respectively. The first two peaks are observed at 7600 m, the third one is at a lower flight level (4600 m). There are no changes in the mercury concentration and the increase in CO coincides with a slight decrease in O_3 during the second observation. The gaps in the CO data are caused by regular automated in-flight-calibration; fortunately the calibrations were performed just before and after crossing the plume.

ACPD
10, 29631–29682, 2010

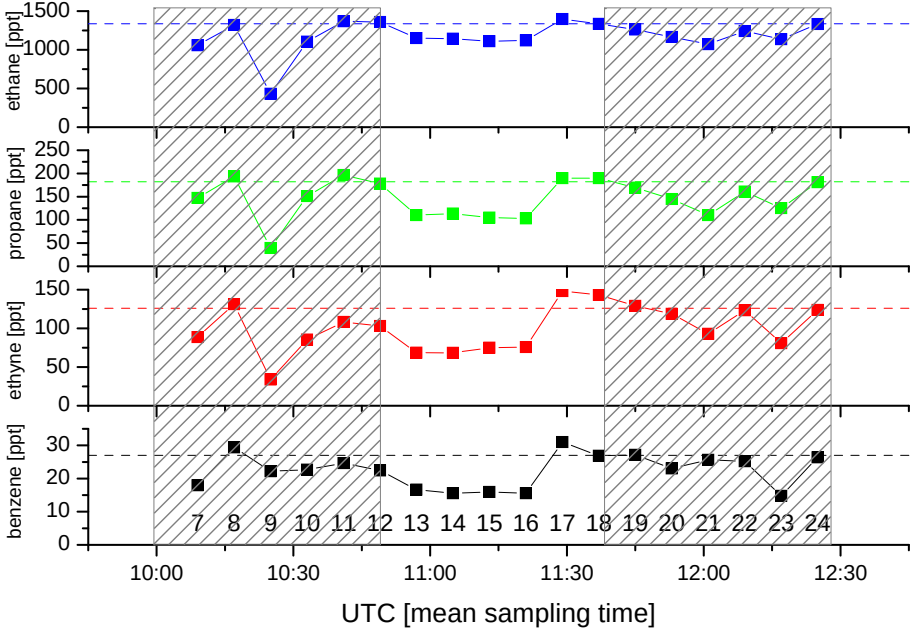

Fig. 10. Hydrocarbons in the plume (hashed areas indicate aerosol samples showing volcanic aerosol, see Fig. 6). In sample No 9 (10:25 UTC) the mixing ratios of ethane, propane and ethyne are strongly reduced, whereas benzene mixing ratios are hardly affected in the volcanic plume.

ACPD
10, 29631–29682, 2010

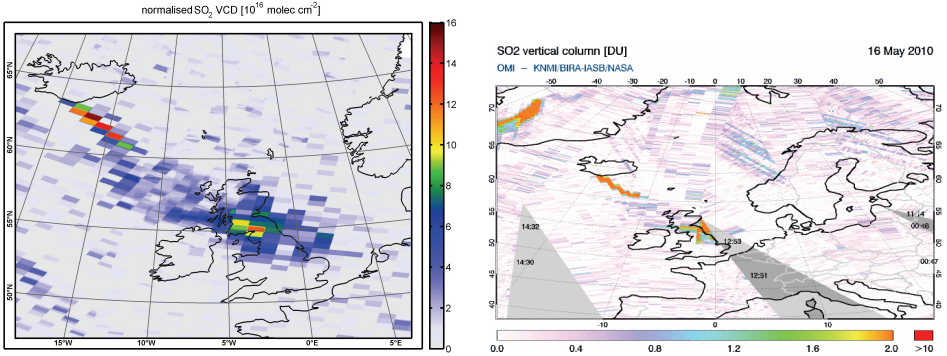

Fig. 11. GOME-2 and OMI (http://www.temis.nl, August 2010) SO_2 vertical column densities on 16 May 2010. While parts of an old plume seem to be moving east over Great Britain, a new one is approaching from Iceland.

ACPD
10, 29631–29682, 2010

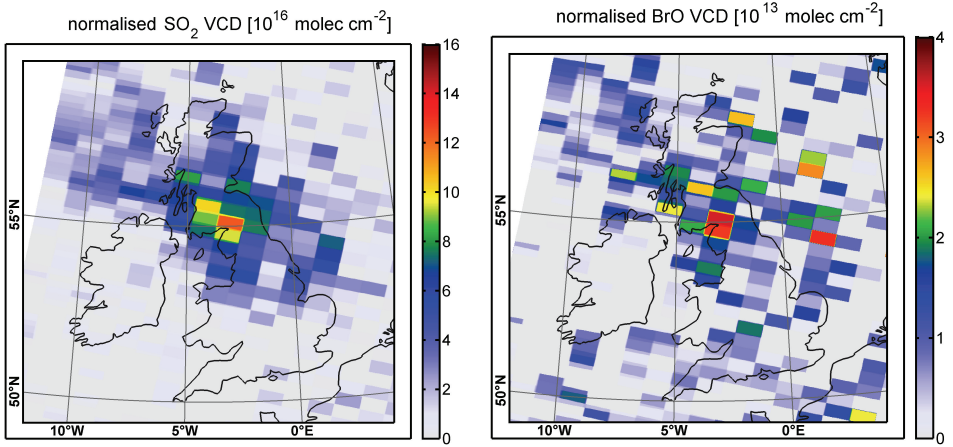

Fig. 12. GOME-2 satellite images showing SO_2 and BrO normalised vertical columns (Sect. 2.3) over the British Isles on 16 May 2010 10:09 UTC. Here only the forward scans are shown, in the overlapping regions the average of the respective VCD is plotted. The main part of the plume is situated over Northern England. But some elevated values are also observed north of Ireland, where the CARIBIC flying laboratory observed the plume.

ACPD
10, 29631–29682, 2010

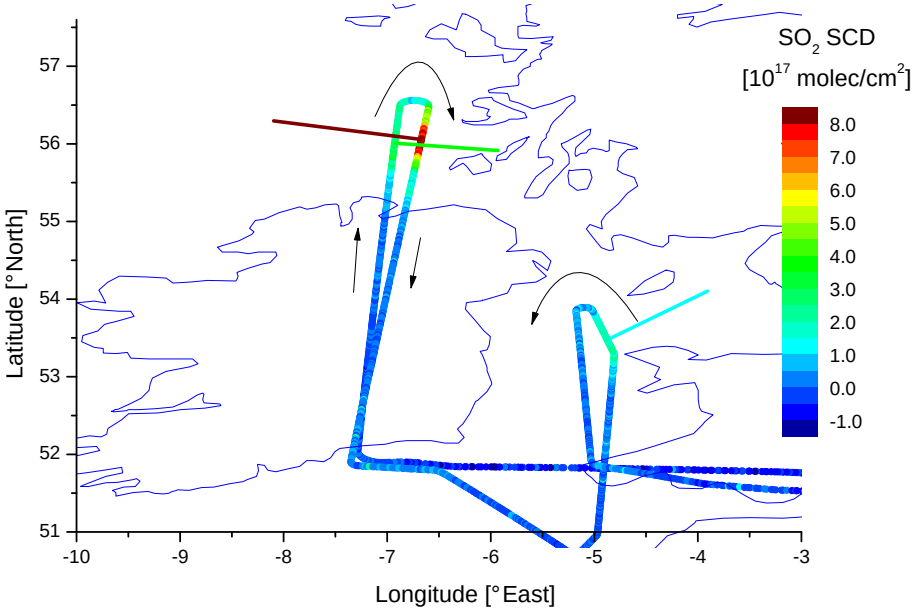

Fig. 13. Viewing direction of the −10° telescope during observations of the SO_2 maxima. The arrows parallel to the flight track indicate the flight direction. The DOAS telescopes are directed to the right. During the first observation of the plume the −10° telescope was pointing east, and 15 min later it was directed to the west.

ACPD
10, 29631–29682, 2010

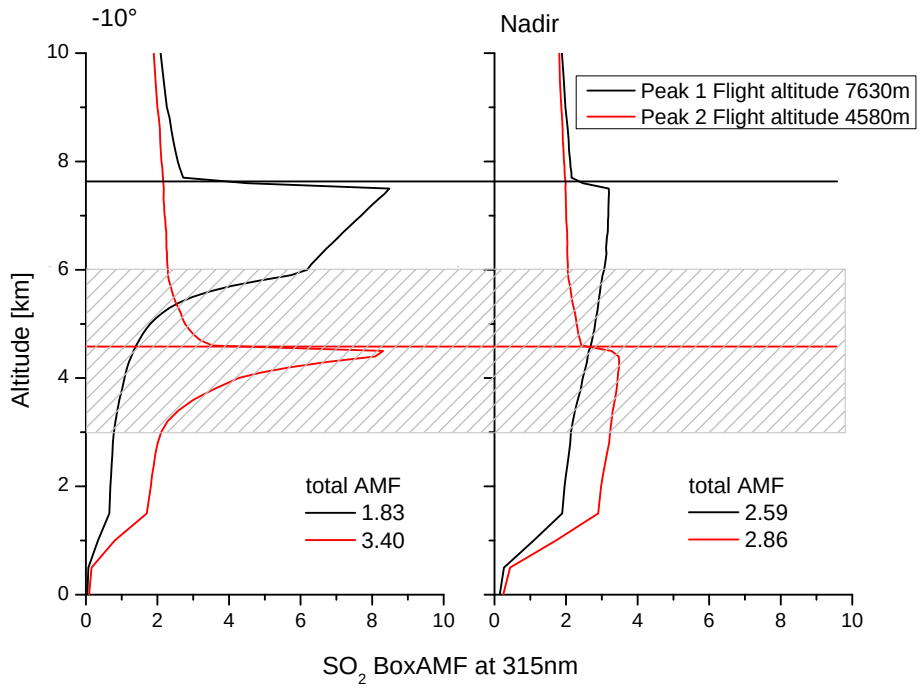

Fig. 14. SO_2 Box AMFs (315 nm) for the viewing geometries used during the plume observations. The strong solid line marks the flight altitude for the respective peak observation. The hatched area indicates the estimated plume altitude range. In the simulations a cloud top height of 1.5 km was assumed, which causes the second rapid decrease in the sensitivity below 1.5 km.

ACPD
10, 29631–29682, 2010

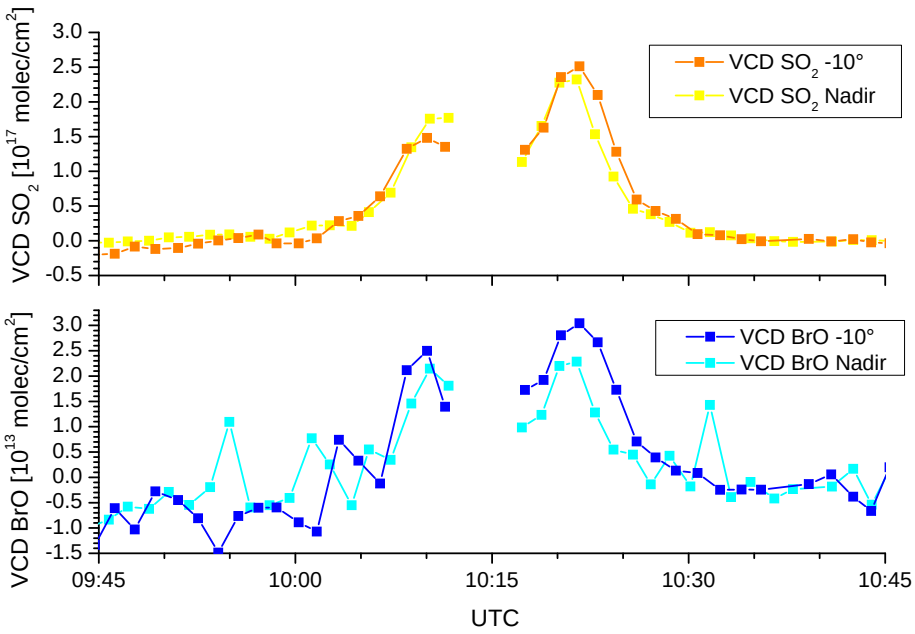

Fig. 15. Vertical column densities for CARIBIC DOAS nadir (yellow, light blue) and −10° (orange, dark blue), only the 80 s averages are shown. The general agreement between the vertical column densities is good.

ACPD
10, 29631–29682, 2010

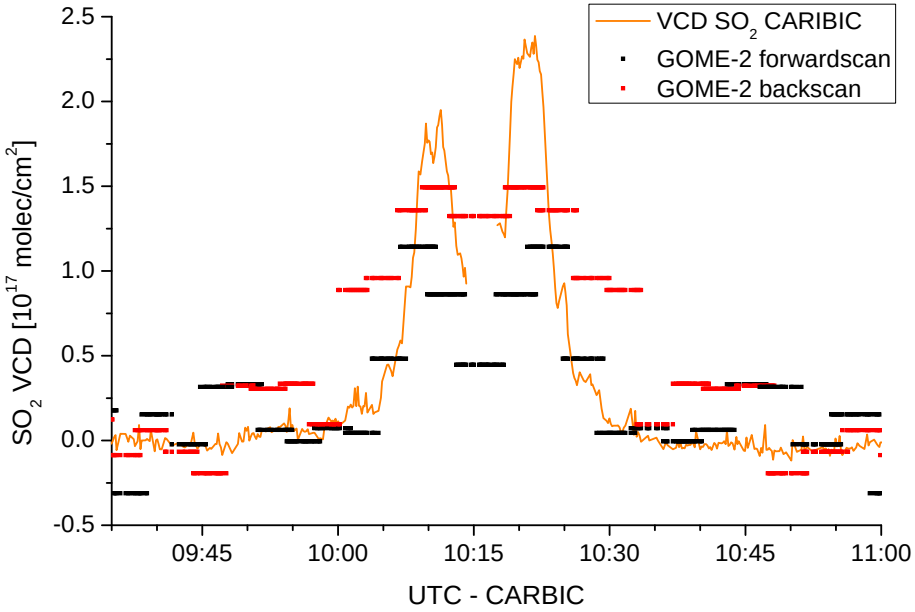

Fig. 16. Comparison of the vertical SO_2 columns, measured by CARIBIC (nadir) and GOME-2. For each CARIBIC DOAS measurement the surrounding pixels (forward and backward scans) are shown. Because the Airbus made a u-turn just north of the plume, the GOME-2 pixels are the same before and after the turn, resulting in the observed symmetry. During the turn the viewing geometry of CARIBIC changed very rapidly, and therefore no AMF were calculated here.

ACPD
10, 29631–29682, 2010

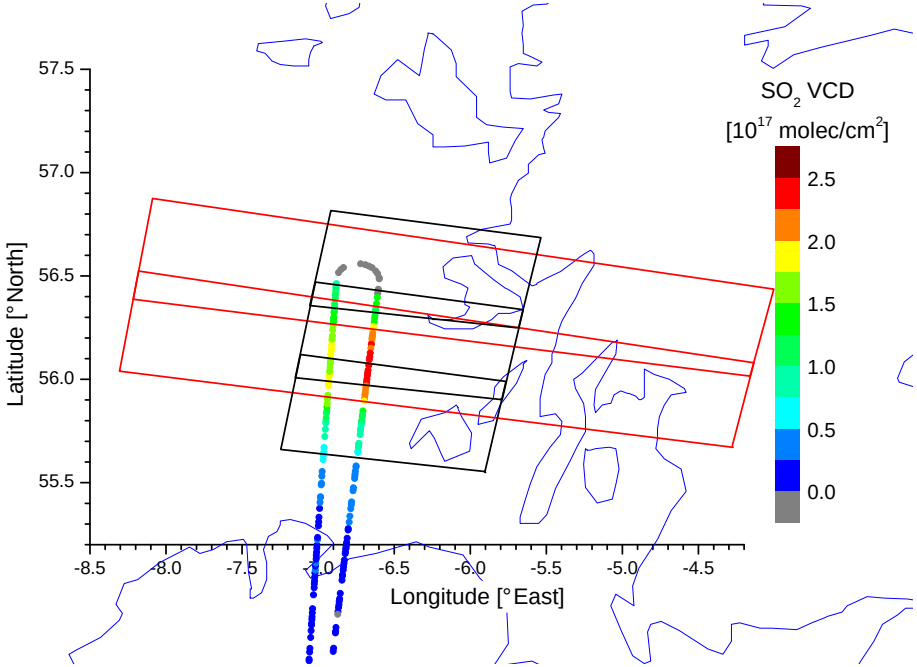

Fig. 17. SO_2 vertical column density from CARIBIC and the observed plume position relative to the GOME-2 pixel (black: forward, red: back scan). In contrast to Fig. 2 only those pixels are shown by which at least one measurement from CARIBIC is covered, being the pixels 21 of swath 26 (North), 27 and 28, as well as the back scan pixel 28 of swath 26 and 27. The maximum of the CARIBIC DOAS SO_2 columns is perfectly covered by one back scan, moreover it is located in the overlapping area of two different forward scan pixels. For the period of the turn no AMF were calcualted, therefore the VCD is grey colour coded.

ACPD
10, 29631–29682, 2010

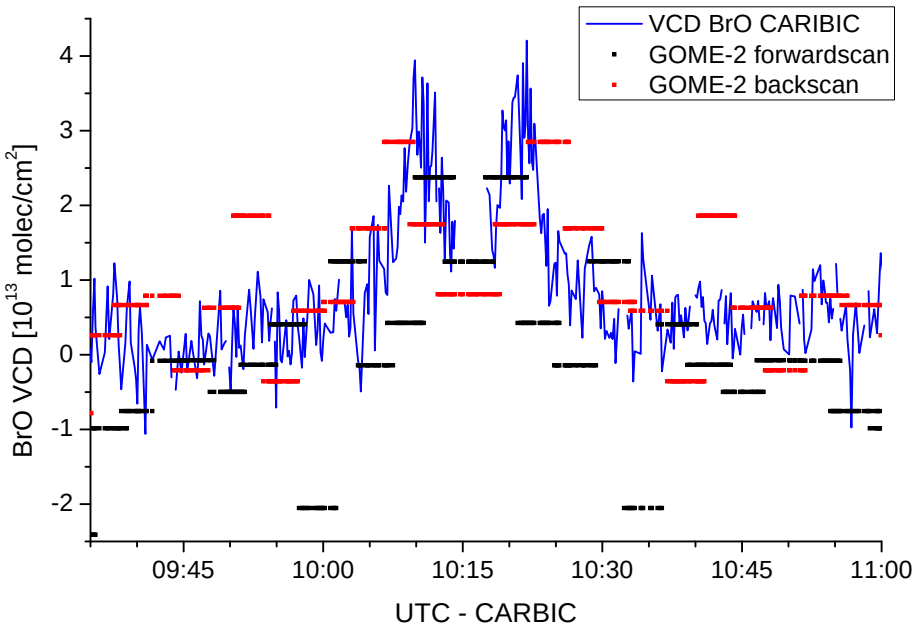

Fig. 18. Comparison of the BrO vertical column densities. Again the structure of the BrO peaks is well found in the GOME-2 data, also the vertical column densities are very similar.

ACPD
10, 29631–29682, 2010